Research Article

Avula Venkateswarlu, Sangapatnam Suneetha, Macherla Jayachandra Babu, Jorige Girish Kumar, Chakravarthula Siva Krishnam Raju, and Qasem Al-Mdallal*

Significance of magnetic field and chemical reaction on the natural convective flow of hybrid nanofluid by a sphere with viscous dissipation: A statistical approach

https://doi.org/10.1515/nleng-2021-0047
Received Oct 05, 2021; accepted Dec 11, 2021

Abstract: Hybrid nanofluid, which is a combination of Propylene Glycol (PG) – Water (H_2O) admixture and paraffin wax and sand, may be utilized as a standby for PG and (H_2O) blend in solar thermal framework. Objective of this article is the exploration of the dissipative flow propylene-glycol and water mixture based hybrid nanofluid by a sphere with chemical reaction and heat source parameters. MATLAB in-built solver bvp4c is utilized to exhibit the impacts of various parameters on regular profiles including temperature. Correlation coefficient is utilized to elucidate the impact of pertinent parameters on engineering parameters of concern, such as, surface friction factor. Main findings of this work are magnetic field is having a negative association with friction factor and chemical reaction is consuming a significant positive relationship with Sherwood number. It is witnessed that heat source and Eckert number are useful to meliorate the fluid temperature. Furthermore, validation is performed among our results and earlier published outcomes. Good agreement is detected.

Keywords: Hybrid nanofluid, sphere, bvp4c, correlation coefficient, magnetic field, chemical reaction, viscous dissipation

Nomenclature

μ	Dynamic viscosity [Kg/ms]
ρ	Density of the fluid [Kg m^{-3}]
β_T	Volumetric coefficient of thermal expansion
a	Radius of the sphere
β_C	Volumetric coefficient of diffusion expansion
g	Acceleration of gravity
υ	Kinematic viscosity [m^2 s^{-1}]
T	Dimensional temperature of fluid [K]
k	Thermal conductivity [W m^{-1}K^{-1}]
C	Dimensional concentration of fluid [mol m^{-3}]
f'	Dimensionless velocity
θ	Dimensionless temperature of fluid
ρc_p	Heat capacity
ψ	Dimensional stream function
u, v	Velocity components in x, y directions [m s^{-1}]
η	Similarity variable
f	Dimensionless Stream function
Φ	Dimensionless concentration of fluid
Gr	Local thermal Grashoff number
Gc	Local diffusion Grashoff number
λ	Buoyancy ratio parameter
Pr	Prandtl number
E_c	Eckert number
S_c	Schmidt number
K_r	Chemical reaction parameter
D_m	Molecular diffusivity [m^2 s^{-1}]
M	Magnetic field parameter
Q_0	Volumetric rate of heat source parameter
k_0	Chemical reaction parameter (dimensional)
ξ	Dimensionless coordinate

***Corresponding Author: Qasem Al-Mdallal:** Department of Mathematical Sciences, United Arab Emirates University, P.O Box 15551, Al Ain, Abu Dhabi, United Arab Emirates; Email: q.almdallal@uaeu.ac.ae
Avula Venkateswarlu, Sangapatnam Suneetha: Department of Applied Mathematics, Yogi Vemana University, Kadapa – 516005, Andhra Pradesh, India
Macherla Jayachandra Babu, Jorige Girish Kumar: Department of Mathematics, S.V.A. Government College, Srikalahasti – 517644, Andhra Pradesh, India
Chakravarthula Siva Krishnam Raju: Department of Mathematics, GITAM School of Science, GITAM University, Bangalore-Campus, Karnataka

1 Introduction

Nanofluids have been introduced as a new interesting kind of heat transfer fluids to replace the use of regular fluids in industrial processes. They may diminish erosion and corrosion significantly owing to their small size. They have a broad range of applications including refrigeration, heat exchangers and cooling of electronic devices. Raju *et al.* [1] considered stretching cylinder and examined the Maxwell fluid flow with Cattaneo-Christov heat flux. Later, various researchers [2–5] assumed stretching sheet as a geometry and theoretically analysed distinct nanofluid flows with different parameters including viscous dissipation. Later, Updhya *et al.* [6–8] scrutinized various nanofluid (including Water + Iron Oxide) flows over varous geometries including moving surface. They detected that the heat transfer rate is high in the presence of ferrous oxide nanoparticles compared to the presence of aluminium oxide nanoparticles in the base fluid. Saba *et al.* [9] discussed the nanofluid (CNT based) flow by a curled elongating surface with heat absorption/generation and detected that the curvature parameter minimizes the friction factor. Durgaprasad *et al.* [10–12] inspected distinct three dimensional nanofluid flows, for instance, water and graphene mixture, across various geometries with different parameters including non-uniform heat source/sink. Sreedevi *et al.* [13] used FEM to solve the mathematical model related to nanofluid (water + Al_2O_3 / water + TiO_2) flow by a wedge with thermal radiation. They observed that there is a reduction in the heat transfer rate for bigger values of radiation parameter. Upadhya *et al.* [14] used the combination of Runge-Kutta and Newton-Raphson procedures to numerically investigate the nanofluid flow among the stationary and porous disks with suction/injection. Eid [15] considered the Riga surface and scrutinized a Darcy-Forchheimer flow of Cu/CMC – Al_2O_3 with heat sink/source. Newly, several researchers [16–18] applied different methods to analyze the various nanofluid flows through distinct geometries. They noticed that the chemical reaction parameter raises the rate of mass transfer and heat transfer rate is high in the absence of magnetic field when compared to its presence. Hybrid nanofluid is a modified version of mono nanofluid, which contains more than one nanoparticle. So, hybrid fluids are having better heat transfer features compared to mono fluids. These are having applications in many areas including solar collectors and military equipment. Ghadikolaei *et al.* [19] studied the shape factor of the nanoparticles in HNF (TiO_2 – Cu/water) flow by an elongating sheet with magnetic field and emphasized that the nanoparticles with platelet shape are more efficient. Tassaddiq *et al.* [20] elucidated the features of mass and heat transfer on the HNF (CNT + Fe_3O_4/H_2O) by a revolving disk with magnetic field and noticed the amelioration in the fluid temperature with the raise in disk rotation. Abbas *et al.* [21] explained a HNF (Ag + Ni/water) flow of two models (Yamada-Ota and Xue) by an elongating cylinder with the aid of bvp4c technique. They observed that the Xue model has less heat transfer rate when compare to other model for temperature gradient. Ahmad and Nadeem [22] considered the upper part of horizontal surface and performed irreversibility analysis in the HNF (MWCNT + SWCNT/water) flow by using the same technique. They noticed that there is an escalation in the entropy with the raise in nanoparticle volume fraction. Later, with the aid of suction and injection, Nadeem *et al.* [23] provided a comparative analysis for the HNF (Cu – Al_2O_3/water) by an exponential curled sheet. Freshly, several researchers [24–28] made contribution to the analysis of hybrid nanofluid flows by considering various geometries.

Fluid flow by a sphere has practical applications in numerous areas of technology, for instance, mineralogy, food engineering and oilfield drilling. Yih [29] inspected the features of heat transfer on the non-Darcy dissipative flow of MHD fluid flow by a sphere immersed in a porous medium. He detected that the heat transfer rate shrinks with bigger Eckert number. Later, Molla *et al.* [30] and Alam *et al.* [31] considered sphere and elucidated the dissipative flow of MHD fluid with heat source. They noticed that the magnetic field parameter minimizes the friction coefficient and Nusselt number minifies with larger heat source parameter. Chamkha *et al.* [32] applied finite difference method to present the analysis of convective flow of a nanofluid through sphere with Brownian motion. Tham *et al.* [33] observed that bioconvection parameters have no significance on temperature in their investigation on the bioconvective flow of nanofluid (water based) through a sphere with thermophoresis. Amanulla *et al.* [34] considered the same geometry and theoretically explained the Darcy-Forchheimer flow of Prandtl-Eyring fluid with slip parameters. Later, Mahdy *et al.* [35] and Alwawi *et al.* [36] scrutinized the nanofluid flow (combined with the Casson fluid) by a sphere with magnetic field. They discovered that the Casson parameter minimizes the fluid velocity and magnetic field parameter enhances the entropy generation. Newly, several researchers [37–42] applied different strategies to examine the features of mass and heat transfer in various nanofluid flows through the sphere.

After cautious perception of the previously mentioned writing, we aim to discuss the significance of the viscous dissipation on the chemically reactive HNF (Propylene glycol – Water mixture + Paraffin Wax + Sand) flow with Ohmic

heating. Results are explicated through plots and a statistical tool named correlation coefficient. Further, validation is performed among the current results and former outcomes and observed a decent accord.

2 Formulation

Natural convective dissipative flow of hybrid nanofluid (Water based Propylene glycol+ Sand + Paraffin Wax) flow by a sphere with Joule heating and chemical reaction is considered. Assumed that the flow is nearby the lower stagnation point of the sphere. Values of the thermophysical attributes of base liquefied and nanomaterials are exhibited in Table 1. Presumptions for this formulation are

(i) Magnetic field of intensiveness B_0 is opposite to flow (y-direction) (see Figure 1).
(ii) $r(x) = a\sin\left(\frac{x}{a}\right)$ is the radial length from symmetric axis to the surface.
(iii) Nanoparticles and base fluid are supposed to be in equilibrium and no slip arises amongst them.
(iv) q_w and s_w are the uniform heat and mass fluxes of the sphere surface.
(v) T_∞, T_w and C_∞, C_w are the surface and ambient fluid temperature and concentrations of the sphere respectively.
(vi) Neglected induced magnetic field.

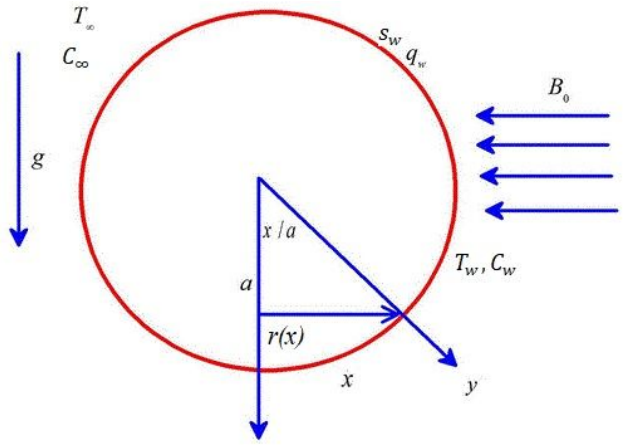

Figure 1: Flow diagram

Flow controlling equations for this problem are characterised as (Alam *et al.* [18]):

$$\frac{\partial(ru)}{\partial x} = -\frac{\partial(rv)}{\partial y}, \tag{1}$$

Table 1: Thermo-physical attributes (Manikandan and Rajan [30])

S. No.		Propylene glycol – Water mixture (f)	Paraffin Wax (ss_1)	Sand (ss_2)
1	ρ (Kg/m^3)	1020	900	2650
2	C_p (J/Kg K)	3342.75	2900	730
3	k (W/m K)	0.363	0.25	1.5

$$u\frac{\partial u}{\partial x} + v\frac{\partial u}{\partial y} - g\beta_T(T - T_\infty)\sin\left(\frac{x}{a}\right) = \mu_{hnf}\frac{\partial^2 u}{\partial y^2} - \frac{\sigma B_0^2}{\rho_{hnf}}u + g\beta_C(C - C_\infty)\sin\left(\frac{x}{a}\right), \tag{2}$$

$$(\rho C_p)_{hnf}\left(u\frac{\partial T}{\partial x} + v\frac{\partial T}{\partial y}\right) = k_{hnf}\frac{\partial^2 T}{\partial y^2} + \mu_{hnf}\left(\frac{\partial u}{\partial y}\right)^2 + Q_0(T - T_\infty) + \sigma B_0^2 u^2, \tag{3}$$

$$u\frac{\partial C}{\partial x} + v\frac{\partial C}{\partial y} = D_m\frac{\partial^2 C}{\partial y^2} - k_0(C - C_\infty), \tag{4}$$

and the conditions are specified as

$$\left.\begin{aligned} &\text{at } y = 0 : u(y) = 0,\ v(y) = 0,\ T(y) = T_w,\ C(y) = C_w \\ &\text{as } y \to \infty : u(y) \to 0,\ T(y) \to T_\infty,\ C(y) \to C_\infty \end{aligned}\right\}. \tag{5}$$

2.1 Thermo physical characteristics of HNF

$$\left.\begin{aligned} (\rho C_p)_{hnf} &= \left[(1-\phi_1)(\rho C_p)_f + \phi_1(\rho C_p)_{ss_1}\right](1-\phi_2) + (\rho C_p)_{ss_2}\phi_2, \\ \mu_{hnf} &= \frac{\mu_f}{\sqrt{(1-\phi_1)^5(1-\phi_2)^5}}, \\ \rho_{hnf} &= \left[(1-\phi_1)\rho_f + \phi_1\rho_{ss_1}\right](1-\phi_2) + \rho_{ss_2}\phi_2, \\ k_{hnf} &= k_{nf} \times \frac{k_{ss_2} + 2k_{nf} - 2k_{nf}\phi_2 + 2k_{ss_2}\phi_2}{k_{ss_2} + 2k_{nf} + k_{nf}\phi_2 - k_{ss_2}\phi_2}, \\ k_{nf} &= k_f \times \frac{k_{ss_1} + 2k_f - 2k_f\phi_1 + 2k_{ss_1}\phi_1}{k_{ss_1} + 2k_f + k_f\phi_1 - k_{ss_1}\phi_1} \end{aligned}\right\}.$$

Following similarity transmutations are used to metamorphose the flow driven equations as a set of ODEs (Alam *et al.* [18]):

$$\left.\begin{aligned} &\xi = \frac{x}{a}, \quad \eta = \frac{y}{a}Gr^{0.25}, \quad \Psi = \upsilon\xi Gr^{0.25}f(\xi,\eta) \\ &\frac{T - T_\infty}{(T_w - T_\infty)} = \theta(\xi,\eta), \quad \frac{C - C_\infty}{(C_w - C_\infty)} = \Phi(\xi,\eta) \end{aligned}\right\}. \tag{6}$$

Here $\Psi$is the stream function, u, v are the constituents of velocity specified by

$$u = r^{-1}\frac{\partial\Psi}{\partial y}, \quad v = -r^{-1}\frac{\partial\Psi}{\partial x}, \tag{7}$$

in order to satisfy the continuity Eq. (1).

With the aid of (6) and (7), Eqs (2–4) are transmuted to:

$$\frac{1}{G_1G_2}f''' - \left(\xi\left(f'\frac{\partial f'}{\partial \xi} - f''\frac{\partial f}{\partial \xi}\right) - ff''(1+\xi\cot\xi) + f'^2\right) + \theta\frac{\mathrm{Sin}\xi}{\xi} - \frac{M}{G_2}f' + \lambda\phi\frac{\mathrm{Sin}\xi}{\xi} = 0, \tag{8}$$

$$\frac{G_3G_{31}}{G_4}\frac{1}{\mathrm{Pr}}\theta'' - \left(\xi\left(f'\frac{\partial \theta}{\partial \xi} - \theta'\frac{\partial f}{\partial \xi}\right) - f\theta'(1+\xi\cot\xi)\right) + \frac{1}{G_1G_4}E_cf'^2 + \frac{Q\theta}{G_4} + ME_cf'^2 = 0, \tag{9}$$

$$\frac{1}{S_c}\phi'' - \left(\xi\left(f'\frac{\partial \phi}{\partial \xi} - \phi'\frac{\partial f}{\partial \xi}\right) - f\phi'(1+\xi\cot\xi)\right) - K_r\phi = 0. \tag{10}$$

Since flow is near the stagnation point of the sphere, $\xi \approx 0$, Eqs (8–10) can be rewritten as:

$$\frac{1}{G_1G_2}f''' + 2ff' - \frac{M}{G_2}f' - f'^2 + \theta + \lambda\phi = 0, \tag{11}$$

$$\frac{G_3G_{31}}{G_4}\frac{1}{Pr}\theta'' + 2f\theta' + \frac{1}{G_3G_4}E_cf''^2 + H\frac{\theta}{G_4} + \frac{1}{G_4}ME_cf'^2 = 0, \tag{12}$$

$$\frac{1}{S_c}\phi'' + 2f\phi' - K_r = 0. \tag{13}$$

On the other hand, conditions in (5) can be rewritten as

$$\left.\begin{aligned}\text{at } \eta = 0 : f(\eta) = 0, f'(\eta) = 0, \Phi(\eta) = 1, \theta(\eta) = 1,\\ \text{as } \eta \to \infty : f'(\eta) \to 0, \Phi(\eta) \to 0\theta(\eta) \to 0,\end{aligned}\right\} \tag{14}$$

where

$$\left.\begin{aligned}G_1 = (1-\phi_2)\left[(1-\phi_1) + \phi_1\frac{\rho_1}{\rho_f}\right] + \phi_{s2}\frac{\rho_2}{\rho_f}, \quad G_2 = (1-\phi_1)^{2.5}(1-\phi_2)^{2.5},\\ G_{31} = \frac{k_1 + 2k_f - 2\phi_1(k_f - k_1)}{k_1 + 2k_f + \phi_1(k_f - k_1)}, \quad G_3 = \frac{k_2 + 2G_{31}k_f - 2\phi_2(G_{31}k_f - k_2)}{k_2 + 2G_{31}k_f + \phi_2(G_{31}k_f - k_2)},\\ G_4 = (1-\phi_2)\left[(1-\phi_1) + \phi_1\frac{(\rho C_p)_1}{(\rho C_p)_f}\right] + \phi_2\frac{(\rho C_p)_2}{(\rho C_p)_f}\end{aligned}\right\}$$

and

$$\left.\begin{aligned}M = \frac{a^2\sigma {B_0}^2}{\rho\upsilon Gr^{0.5}}, \quad \lambda = \frac{Gc}{Gr}, \quad Gc = \frac{g\beta_c(C_w - C_\infty)a^3}{\upsilon^2}, \quad \mathrm{Pr} = \frac{\mu C_p}{k},\\ E_c = \frac{\left(\upsilon\sqrt{Gr}\right)^2}{a^2C_p(T_w - T_\infty)}, \quad S_c = \frac{\upsilon}{D_m}, \quad K_r = \frac{k_0a^2}{\upsilon Gr^{0.5}}, \quad H = \frac{Q_0a^2}{\upsilon\rho C_pGr^{0.5}}\end{aligned}\right\}$$

2.2 Physical parameters

Surface drag force is defined as:

$$C_{f_x} = \frac{Gr^{-\frac{3}{4}}a^2}{\mu\upsilon}\tau_w, \tag{15}$$

where $\tau_w = \mu_{hnf}\left(\frac{\partial u}{\partial y}\right)\Big|_{y=0}$. By using (6) and (7), we may rewrite (15) as

$$C_{f_x} = \frac{1}{G_1}\xi f''(\xi, 0).$$

Formulae to find transfer rates (heat and mass) are chosen as:

$$Nu = \frac{aGr^{-\frac{1}{4}}}{k_f(T_w - T_\infty)}q_w, \quad Sh = \frac{aGr^{-\frac{1}{4}}}{D_m(C_w - C_\infty)}S_w, \tag{16}$$

where (wall heat flux) $q_w = -k_{hnf}\frac{\partial T}{\partial y}\Big|_{y=0}$, (wall mass flux) $s_w = -D_m\frac{\partial C}{\partial y}\Big|_{y=0}$.

With the aid of (6) and (7), formulae in (16) are rewritten as:

$$Nu = -G_3G_{31}\theta'(\xi, 0), \quad \text{and} \quad Sh = -\Phi'(\xi, 0).$$

3 Numerical Procedure

MATLAB built-in function bvp4c is used to resolve the altered Eqs (11–13) with the conditions (14). Since bvp4c solver is built-in function, it is simple to use this function.

As a pre-process to write the code, first we need to adopt the following assumptions (Waini *et al.* [31]):

$$z_1 = f, \quad z_3 = f'', \quad z_2 = f', \quad z_5 = \theta',$$
$$z_4 = \theta, \quad z_7 = \Phi', \quad z_6 = \Phi.$$

Then, using the Eqs (11–13) with conditions (14), we can develop a subsequent system of ODEs of first order:

$$\left.\begin{aligned} z_1' &= z_2, \\ z_2' &= z_3, \\ z_3' &= -G_1 G_2 \left(2 z_1 z_2 - \frac{M}{G_2} z_2 - z_2^2 + z_4 + \lambda z_6\right) \\ z_4' &= z_5, \\ z_5' &= -\frac{G_4}{G_3 G_{31}} \\ &\cdot \Pr \left(2 z_1 z_5 + \frac{1}{G_3 G_4} E_c z_3^2 + H \frac{z_4}{G_4} + \frac{1}{G_4} M E_c z_2^2\right) \\ z_6' &= z_7, \\ z_7' &= -S_c \left(2 z_1 z_7 - K_r\right) \end{aligned}\right\} \quad (17)$$

with the conditions

$$\left.\begin{aligned} za(1) &= 0, \\ za(2) = 0, \quad za(4) &= 1, \quad za(6) = 1 \\ zb(2) = 0, \quad zb(4) &= 0, \quad zb(6) = 0 \end{aligned}\right\}. \quad (18)$$

After converting the above system as a MATLAB code, we can execute it to get the required outcomes in the form of graphs.

4 Interpretation of results

In this study, outcomes are offered for two cases i.e., PG – Water + Paraffin Wax + Sand and PG – Water + Paraffin Wax.

4.1 Velocity profiles

When we raise the volume fraction of nanoparticle, there is an escalation in the viscosity of the fluid, which obstructs the fluid flow. So, velocity minifies with the larger ϕ_1 (Figure 2). Fluid particles try to change their direction within the sight of magnetic field. Consequently, fluid velocity diminishes (Figure 3). Figure 4 exhibits the natural behaviour (increment) of buoyancy ratio parameter on velocity profile.

4.2 Temperature profiles

When E_c increases, there is a change of increment in internal friction of the fluid. Due to that reason, fluid temperature upsurges (Figure 5). Figure 6 elucidated the impact of ϕ_1 on temperature field. It is perceived that temperature ameliorates with the raise in ϕ_1. This may be due to

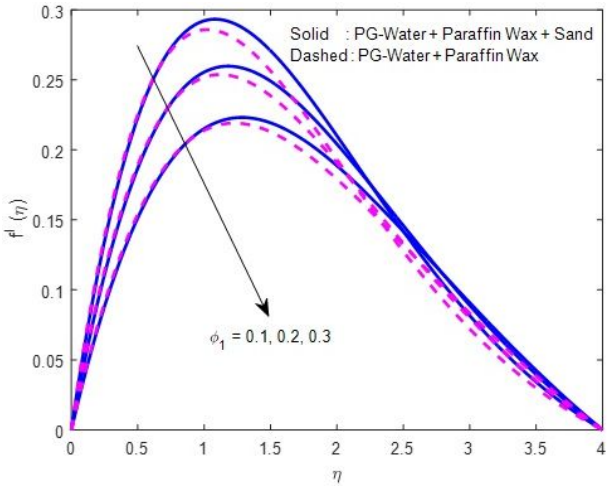

Figure 2: Outcome of ϕ_1 on f'

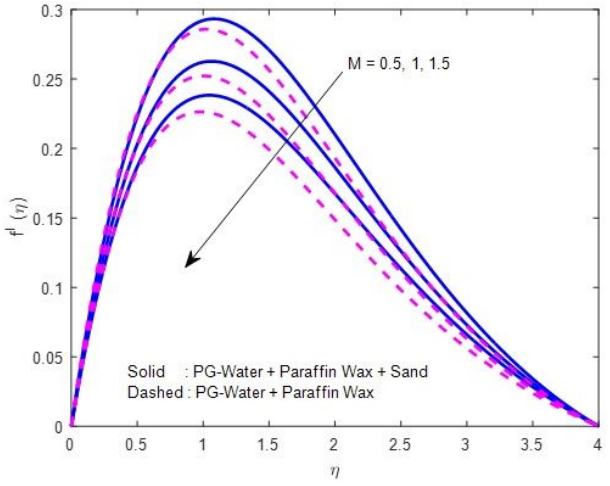

Figure 3: Outcome of M on f'

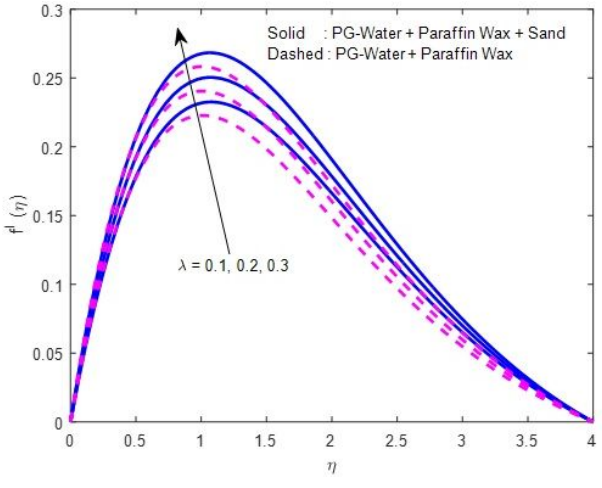

Figure 4: Outcome of λ on $f'(\eta)$

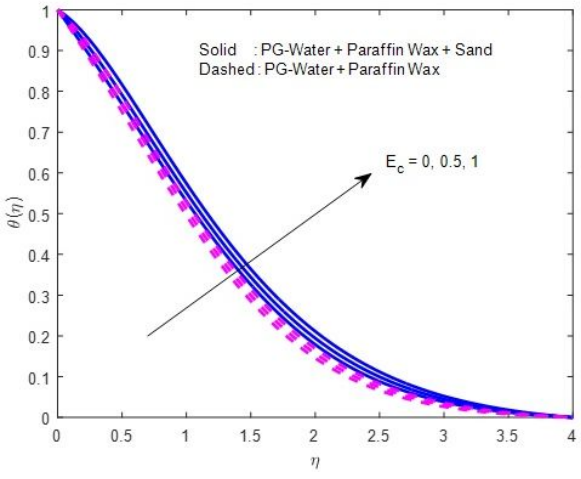

Figure 5: Outcome of E_c on θ

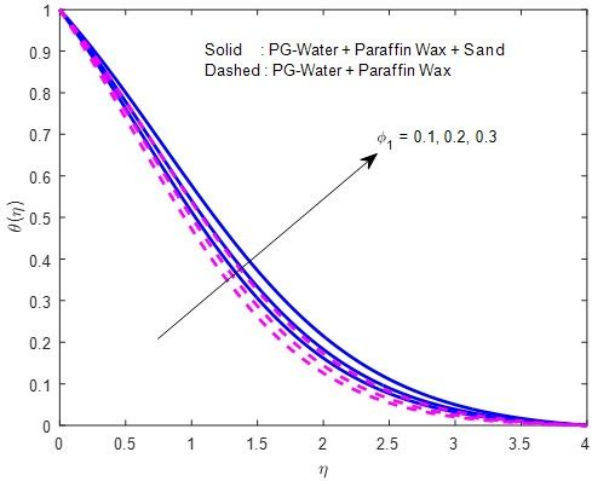

Figure 6: Outcome of ϕ_1 on θ

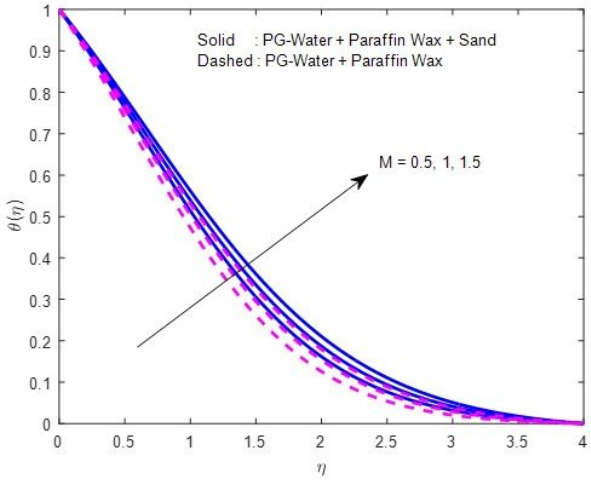

Figure 7: Outcome of M on θ

the reason that larger ϕ_1 adds more viscosity to the fluid, which in turn, enhances the friction between the particles. Raise in magnetic field parameter ameliorates the rate at which linear momentum is transferred from the electromagnetic field to the fluid particle. That means, there is an increase in the energy transfer from electromagnetic field to the fluid particle. So, enrichment in temperature observes with larger magnetic field parameter (Figure 7). Figure 8 displays the fact that the larger H raises the temperature profile. Usually, larger heat source parameter causes proliferation of additional heat within the fluid and in turn, assists to enhance the wideness of the thermal boundary.

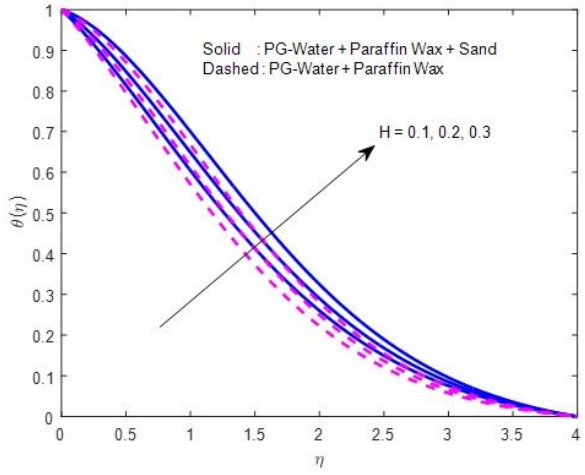

Figure 8: Outcome of H on $\theta(\eta)$

4.3 Concentration profiles

Mass diffusivity minifies with larger Schmidt number. So, concentration minifies with larger Schmidt number (Figure 9). Typically, with the step-up in chemical reaction parameter, concentration decreases (Figure 10). More entropy generation may be the reason for this behaviour.

4.4 Study of surface drag force and transfer rates (heat, mass)

Figures 11–12 emphasized that M minifies the surface drag force and ϕ_1 escalates the same. Larger values of E_c and H led to the lessening in the thermal boundary layer thinness. That means, they minify the heat transfer rate (Figures 13–14). From Figures 15–16, it is detected that Sc, Γ ameliorate the mass transfer rate. This may be due to reason that Sc, Γ minimize the concentration boundary layer thickness.

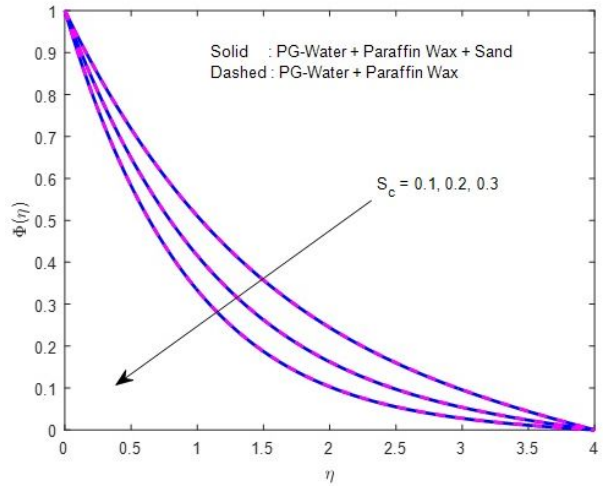

Figure 9: Effect of S_c on $\Phi(\eta)$

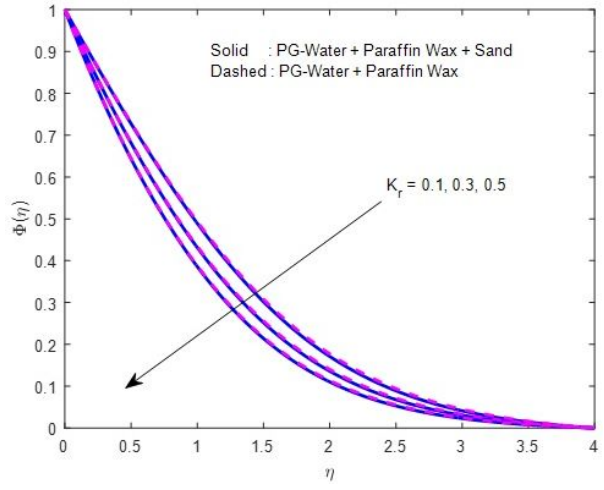

Figure 10: Effect of K_r on $\Phi(\eta)$

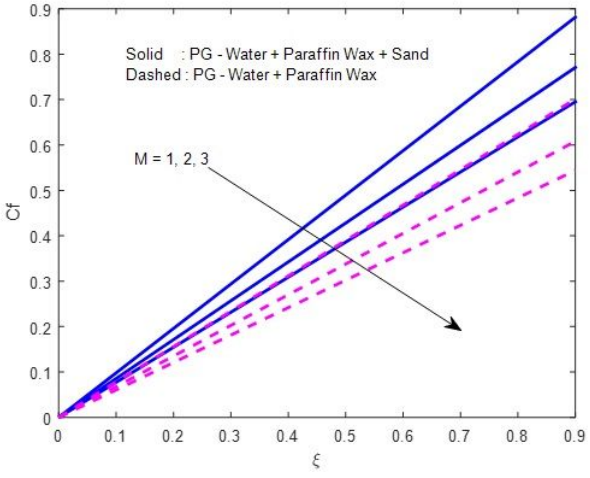

Figure 11: Impression of M on surface drag force (Cf)

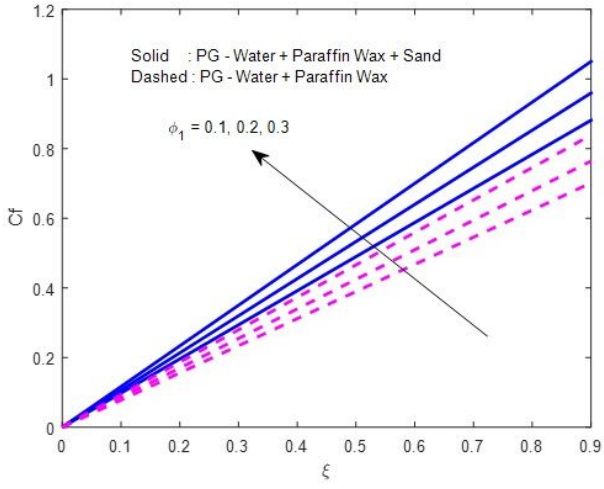

Figure 12: Impression of ϕ_1 on Cf

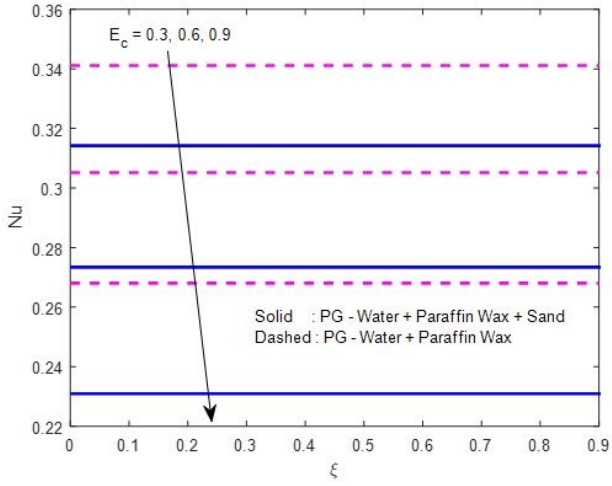

Figure 13: Impression of E_c on Nusselt number (Nu)

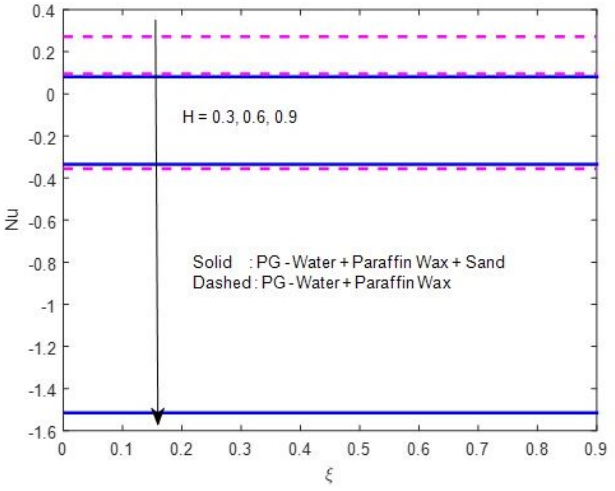

Figure 14: Impression of H on Nu

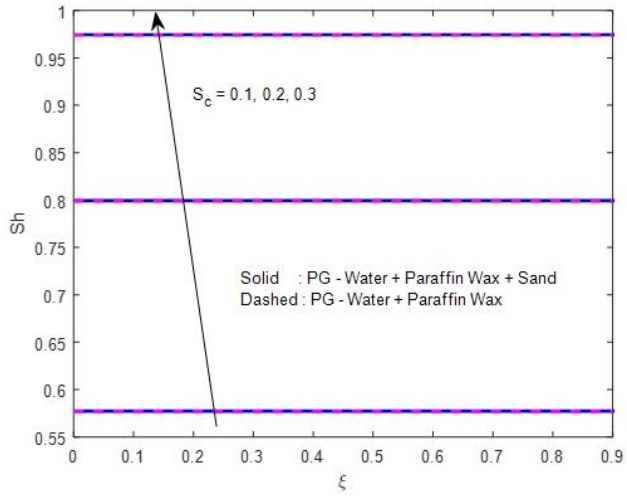

Figure 15: Impression of S_c on Sherwood number (Sh)

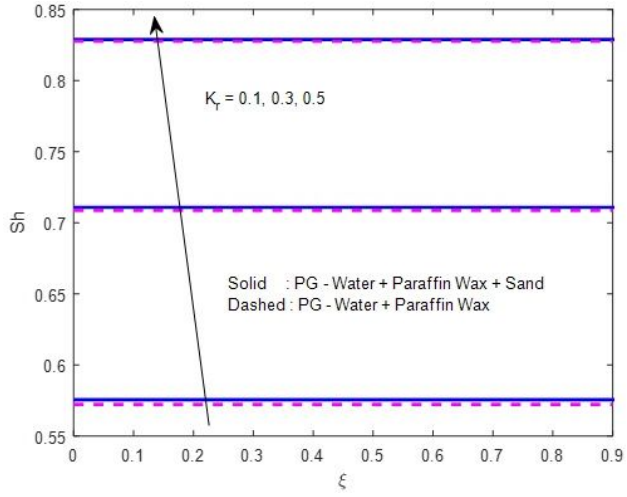

Figure 16: Impression of K_r on Sh

4.5 Correlation coefficient and its significance

We have done a statistical analysis by using correlation coefficient to confirm the results related to physical parameters, such as, surface drag force.

The Coefficient is a numerical quantity of relationship in the midst of two elements. Worth of the measurement lies among +1 and −1 where former represents positive affiliation and latter represents negative affiliation.

$$r_{yz} = \frac{p\left(\sum_{i=1}^{p} y_i z_i\right) - \left(\sum_{i=1}^{p} y_i\right)\left(\sum_{i=1}^{p} z_i\right)}{\sqrt{\left[p\sum_{i=1}^{p} y_i - \left(\sum_{i=1}^{p} y_i\right)^2\right]}\sqrt{\left[p\sum_{i=1}^{p} z_i - \left(\sum_{i=1}^{p} z_i\right)^2\right]}}$$

is the expression to assess the correlation coefficient for two variables y and z.

P.E (Probable Error) of correlation coefficient helps with choosing the exactness and reliability of the coefficient value. Correlation between y and z is significant if $\frac{|r_{yz}|}{P_E} > 6$ (or $|r_{yz}| > 6P_E$) and unimportant otherwise.

$P_E = 0.6745\frac{1-r_{yz}^2}{\sqrt{p}}$ is the expression to assess the Probable Error.

From Table 2, it is clear that magnetic field parameter is consuming a noteworthy negative relationship with surface drag force and the volume fraction parameter of nanoparticle is consuming a positive affiliation with the same parameter. Table 3 revealed the fact that there is a negative association between E_c and heat transfer rate. And also, it is clear that the impact of M is same as E_c on the Nusselt number. Further, it is detected that there is a substantial positive affiliation between Sherwood number and Schmidt number (Table 4).

Table 2: Association among parameters and surface drag force

	Cf		
	PG − Water + Paraffin Wax + Sand		
	r_{yz}	P_E	$\frac{\lvert r_{yz}\rvert}{P_E}$
M	−0.9956	0.001292	770.59
ϕ_1	0.9983	0.000500	1996
	Cf		
	PG − Water + Paraffin Wax		
	r_{yz}	P_E	$\frac{\lvert r_{yz}\rvert}{P_E}$
M	−0.9950	0.001468	677.79
ϕ_1	0.9990	0.000294	3397.96

Table 3: Association among parameters and heat transfer rate

	Nu		
	PG − Water + Paraffin Wax + Sand		
	r_{yz}	P_E	$\frac{\lvert r_{yz}\rvert}{P_E}$
E_c	−0.9999	0.000029	34479.31
H	−0.9986	0.000412	2423.79
	Nu		
	PG − Water + Paraffin Wax		
	r_{yz}	P_E	$\frac{\lvert r_{yz}\rvert}{P_E}$
E_c	−0.9999	0.000029	34479.31
H	−0.9986	0.000412	2423.79

Table 4: Association among parameters and mass transfer rate

	Sh					
	PG – Water + Paraffin Wax + Sand			PG – Water + Paraffin Wax		
	r_{yz}	P_E	$\frac{\lvert r_{yz}\rvert}{P_E}$	r_{yz}	P_E	$\frac{\lvert r_{yz}\rvert}{P_E}$
S_c	0.9997	0.000088	11360.23	0.9997	0.000088	11360.23
K_r	0.9999	0.000029	34479.31	0.9999	0.000029	34479.31

4.6 Validation

Validation is performed among our results and formerly published outcomes. We saw an acceptable concord (See Table 5).

Table 5: Validation of present results with earlier outcomes for Cf and Nu

ξ	$H = 0.10$			
	Alam *et al.* [18]		Present Results	
	Cf	Nu	Cf	Nu
0	0.00000	0.84401	0.000000	0.844055
$\pi/18$	0.16143	0.62483	0.161447	0.624855
$\pi/9$	0.31993	0.61026	0.319918	0.610279
$\pi/6$	0.47266	0.59539	0.472573	0.595446
$2\pi/9$	0.61686	0.57701	0.616897	0.577045

5 Conclusion

Hybrid nanofluid, which is a combination of Propylene Glycol (PG) – Water (H_2O) admixture and paraffin wax and sand, may be utilized as a standby for PG and H_2O blend in solar thermal framework. With these things in mind, investigation is done on the dissipative flow propylene-glycol and water mixture based hybrid nanofluid by a sphere with chemical reaction and heat source parameters. MATLAB inbuilt simulator bvp4c is enforced to solve the transmuted classification of equations. Correlation coefficient is utilized to elucidate the impact of pertinent parameters on engineering parameters of concern, such as, surface friction factor. Additionally, we have verified the current results with the earlier outcomes and saw a decent concord. Primary conclusions of this study are displayed underneath:

- Velocity minifies with bigger ϕ_1.
- Buoyancy ratio parameter meliorates the fluid velocity.
- minimizes the friction factor.
- E_c and H are useful to enhance the thermal boundary thickness. So, Nusselt number minifies with the raise in those parameters.
- Sherwood Number is consuming a generous positive affiliation with Schmidt number.

Funding information: The authors state no funding involved.

Author contributions: All authors have accepted responsibility for the entire content of this manuscript and approved its submission.

Conflict of interest: The authors state no conflict of interest.

References

[1] Raju CS, Kumar RK, Varma SV, Madaki AG, Prasad PD. Transpiration effects on MHD flow over a stretched cylinder with Cattaneo–Christov heat flux with suction or injection. Arab J Sci Eng. 2018;43(5):2273–80.

[2] Sivakumar N, Prasad PD, Raju CS, Varma SV, Shehzad SA. Partial slip and dissipation on MHD radiative ferro-fluid over a non-linear permeable convectively heated stretching sheet. Results Phys. 2017;7:1940–9.

[3] Upadhay MS, Raju CS. Cattaneo-Christov on heat and mass transfer of unsteady Eyring Powell dusty nanofluid over sheet with heat and mass flux conditions. Inform Med Unlocked. 2017;9:76-85. https://doi.org/10.1016/j.imu.2017.06.001.

[4] Nagendramma V, Kumar RK, Prasad PD, Leelaratnam A, Varma SV. Themodiffusion effects on MHD boundary layer slip flow of nanofluid over a nonlinear stretching sheet through a porous medium. J Porous Media. 2017;20(11):961–70.

[5] Prasad PD, Raju CS, Varma SV, Shehzad SA, Madaki AG. Cross diffusion and multiple slips on MHD Carreau fluid in a suspension of microorganisms over a variable thickness sheet. J Braz Soc Mech Sci Eng. 2018;40(5):1–3.

[6] Upadhya SM, Raju CS, Shehzad SA, Abbasi FM. Flow of Eyring-Powell dusty fluid in a deferment of aluminum and ferrous oxide nanoparticles with Cattaneo-Christov heat flux. Powder Technol. 2018;340:68–76.

[7] Upadhya SM, Raju CS, Saleem S. Nonlinear unsteady convection on micro and nanofluids with Cattaneo-Christov heat flux.

Results Phys. 2018;9:779–86.
[8] Upadhya SM, Raju CS. Comparative study of Eyring and Carreau fluids in a suspension of dust and nickel nanoparticles with variable conductivity. Eur Phys J Plus. 2018;133(4):1–5.
[9] Saba F, Ahmed N, Hussain S, Khan U, Mohyud-Din ST, Darus M. Thermal analysis of nanofluid flow over a curved stretching surface suspended by carbon nanotubes with internal heat generation. Appl Sci (Basel). 2018;8(3):395.
[10] Prasad PD, Varma SV, Raju CS, Shehzad SA, Meraj MA. 3D flow of Carreau polymer fluid over variable thickness sheet in a suspension of microorganisms with Cattaneo-Christov heat flux. Rev Mex Fis. 2018;64(5):519–29.
[11] Prasad PD, Varma SV, Hoque MM, Raju CS. Combined effects of Brownian motion and thermophoresis parameters on three-dimensional (3D) Casson nanofluid flow across the porous layers slendering sheet in a suspension of graphene nanoparticles. Neural Comput Appl. 2019;31(10):6275–86.
[12] Prasad PD, Saleem S, Varma SV, Raju CS. Three dimensional slip flow of a chemically reacting Casson fluid flowing over a porous slender sheet with a non-uniform heat source or sink. J Korean Phys Soc. 2019;74(9):855–64.
[13] Sreedevi P, Reddy PS, Sheremet M. A comparative study of Al2O3 and TiO2 nanofluid flow over a wedge with non-linear thermal radiation. Int J Numer Methods Heat Fluid Flow. 2019;30(3):1291–317.
[14] Upadhya SM, Devi RR, Raju CS, Ali HM. Magnetohydrodynamic nonlinear thermal convection nanofluid flow over a radiated porous rotating disk with internal heating. J Therm Anal Calorim. 2021;143(3):1973–84.
[15] Eid MR. Thermal characteristics of 3D nanofluid flow over a convectively heated Riga surface in a Darcy–Forchheimer porous material with linear thermal radiation: an optimal analysis. Arab J Sci Eng. 2020;45(11):9803–14.
[16] Kumar SG, Prasad PD, Raju CS, Shehzad SA, Bashir MN, Varma SV. Three-dimensional magnetized slip flow of Carreau non-Newtonian fluid flow through conduction and radiative chemical reaction. Indian J Phys. 2021.
[17] Saranya S, Al-Mdallal QM. Computational study on nanoparticle shape effects of Al2O3-silicon oil nanofluid flow over a radially stretching rotating disk. Case Stud Therm Eng. 2021;25:100943.
[18] Gowda RP, Al-Mubaddel FS, Kumar RN, Prasannakumara BC, Issakhov A, Rahimi-Gorji M, et al. Computational modelling of nanofluid flow over a curved stretching sheet using Koo–Kleinstreuer and Li (KKL) correlation and modified Fourier heat flux model. Chaos Solitons Fractals. 2021;145:110774.
[19] Ghadikolaei SS, Yassari M, Sadeghi H, Hosseinzadeh K, Ganji DD. Investigation on thermophysical properties of Tio2–Cu/H2O hybrid nanofluid transport dependent on shape factor in MHD stagnation point flow. Powder Technol. 2017;322:428–38.
[20] Tassaddiq A, Khan S, Bilal M, Gul T, Mukhtar S, Shah Z, et al. Heat and mass transfer together with hybrid nanofluid flow over a rotating disk. AIP Adv. 2020;10(5):055317.
[21] Abbas N, Nadeem S, Saleem A, Malik MY, Issakhov A, Alharbi FM. Models base study of inclined MHD of hybrid nanofluid flow over nonlinear stretching cylinder. Chin J Phys. 2021;69:109–17.
[22] Ahmad S, Nadeem S. Application of CNT-based micropolar hybrid nanofluid flow in the presence of Newtonian heating. Appl Nanosci. 2020;10(12):5265–77.
[23] Nadeem S, Abbas N, Malik MY. Inspection of hybrid based nanofluid flow over a curved surface. Comput Methods Programs Biomed. 2020 Jun;189:105193.
[24] Geridönmez BP, Öztop HF. Effects of inlet velocity profiles of hybrid nanofluid flow on mixed convection through a backward facing step channel under partial magnetic field. Chem Phys. 2021;540:111010.
[25] Al-Hossainy AF, Eid MR. Combined experimental thin films, TDDFT-DFT theoretical method, and spin effect on [PEG-H2O/ZrO2+ MgO] hybrid nanofluid flow with higher chemical rate. Surf Interfaces. 2021;23:100971.
[26] Alizadeh R, Abad JM, Ameri A, Mohebbi MR, Mehdizadeh A, Zhao D, et al. A machine learning approach to the prediction of transport and thermodynamic processes in multiphysics systems-heat transfer in a hybrid nanofluid flow in porous media. J Taiwan Inst Chem Eng. 2021;124:1–17.
[27] Anuar NS, Bachok N, Pop I. Influence of buoyancy force on Ag-MgO/water hybrid nanofluid flow in an inclined permeable stretching/shrinking sheet. Int Commun Heat Mass Transf. 2021;123:105236.
[28] Jamaludin A, Nazar R, Naganthran K, Pop I. Mixed convection hybrid nanofluid flow over an exponentially accelerating surface in a porous media. Neural Comput Appl. 2021;33(22):1–1.
[29] Yih KA. Viscous and Joule heating effects on non-Darcy MHD natural convection flow over a permeable sphere in porous media with internal heat generation. Int Commun Heat Mass Transf. 2000;27(4):591–600.
[30] Molla MM, Hossain MA, Taher MA. Magnetohydrodynamic natural convection flow on a sphere with uniform heat flux in presence of heat generation. Acta Mech. 2006;186(1):75–86.
[31] Alam MM, Alim MA, Chowdhury MM. Viscous dissipation effects on MHD natural convection flow over a sphere in the presence of heat generation. Nonlinear Anal (Vilnius). 2007;12(4):447–59.
[32] Chamkha A, Gorla RS, Ghodeswar K. Non-similar solution for natural convective boundary layer flow over a sphere embedded in a porous medium saturated with a nanofluid. Transp Porous Media. 2011;86(1):13–22.
[33] Tham L, Nazar R, Pop I. Mixed convection flow over a solid sphere embedded in a porous medium filled by a nanofluid containing gyrotactic microorganisms. Int J Heat Mass Transf. 2013;62:647–60.
[34] Amanulla CH, Saleem S, Wakif A, AlQarni MM. MHD Prandtl fluid flow past an isothermal permeable sphere with slip effects. Case Stud Therm Eng. 2019;14:100447.
[35] Mahdy A, Chamkha AJ, Nabwey HA. Entropy analysis and unsteady MHD mixed convection stagnation-point flow of Casson nanofluid around a rotating sphere. Alex Eng J. 2020;59(3):1693–703.
[36] Alwawi FA, Alkasasbeh HT, Rashad AM, Idris R. MHD natural convection of Sodium Alginate Casson nanofluid over a solid sphere. Results Phys. 2020;16:102818.
[37] Salahuddin T, Sakinder S, Alharbi SO, Abdelmalek Z. A brief comparative study of gamma alumina–water and gamma alumina–EG nanofluids flow near a solid sphere. Math Comput Simul. 2021;181:487–500.
[38] Mahdy AE, Hady FM, Nabwey HA. Unsteady homogeneous-heterogeneous reactions in MHD nanofluid mixed convection flow past a stagnation point of an impulsively rotating sphere. Therm Sci. 2021;25 1 Part A:243–56.
[39] Ghani M, Rumite W. Keller-Box scheme to mixed convection flow over a solid sphere with the effect of MHD. MUST: J Math Educ Sci Technol. 2021;6(1):97–120.

[40] EL-Kabeir S. Rashad A, Khan W, Abdelrahman ZM. Micropolar ferrofluid flow via natural convective about a radiative isoflux sphere. Adv Mech Eng. 2021;13(2):1687814021994392.
[41] Mohamed RA, Hady FM, Mahdy A, Abo-zai OA. Laminar MHD natural convection flow due to non-Newtonian nanofluid with dust nanoparticles around an isothermal sphere: non-similar solution. Phys Scr. 2021;96(3):035215.
[42] Jenifer AS, Saikrishnan P, Lewis RW. Unsteady MHD Mixed Convection Flow of Water over a Sphere with Mass Transfer. J Appl Comput Mech. 2021;7(2):935–43.
[43] Hanif H, Khan I, Shafie S. Heat transfer exaggeration and entropy analysis in magneto-hybrid nanofluid flow over a vertical cone: a numerical study. J Therm Anal Calorim. 2020;141(5):2001–17.
[44] Manikandan S, Rajan KS. New hybrid nanofluid containing encapsulated paraffin wax and sand nanoparticles in propylene glycol-water mixture: potential heat transfer fluid for energy management. Energy Convers Manage. 2017;137:74–85.
[45] Waini I, Ishak A, Pop I. Hybrid nanofluid flow past a permeable moving thin needle. Mathematics. 2020;8(4):612.